Combustion and Flame 240 (2022) 111988

Contents lists available at ScienceDirect

Combustion and Flame

journal homepage: www.elsevier.com/locate/combustflame

On the hot surface ignition of a wall-stagnating spray flame

Danyal Mohaddes*, Matthias Ihme

Department of Mechanical Engineering, Stanford University, California, USA 94305

ARTICLE INFO

Article history:
Received 6 September 2021
Revised 6 January 2022
Accepted 6 January 2022

Keywords:
Hot surface ignition
Spray ignition
Flame-wall interaction

ABSTRACT

The ignition of fuel sprays due to interaction with hot surfaces is an important phenomenon in the safety analysis of many engineering systems. We perform a parametric study of the hot surface ignition (HSI) of a fuel spray approaching a heated surface caused by the accidental leakage of a fuel line. To this end, we employ a one-dimensional Eulerian-Eulerian formulation with a non-equilibrium evaporation model and a realistic chemical mechanism to describe *n*-dodecane fuel chemistry. We first describe and analyze the phenomenology of the unsteady processes leading to ignition using non-dimensionalized quantities. Through consideration of the temporal development of the most reactive mixture, we demonstrate that ignition occurs at a fuel-lean composition in a premixed region near the hot surface. Using non-dimensional parameters identified from the governing equations, we perform a parametric study of the time, location and local mixture composition at ignition and determine the ignition limits. We then identify the most important parametric sensitivities for physical analysis using a data-driven classification method. Our analysis demonstrates a contraction of the ignition limits with increased Stokes number and a regime of parametric insensitivity of igniting mixture composition. We also show that at high Damköhler numbers, the ignition location conforms to the parametric behavior of the thermal boundary layer, whereas at low Damköhler numbers approaching the ignition limit it reaches a near-unity value of the quenching Peclet number. We then compare the demonstrated parametric dependencies to the results of the quasi-steady asymptotic ignition literature, showing that our results are consistent with those obtained analytically within the limitations imposed by the simplified formulation of the latter.

1. Introduction

In many engineering settings, including the automotive, aerospace, chemical and petroleum industries, liquid fuel is supplied through pressurized lines near hot components. Accidental ignition is a key safety concern in such cases, since a localized structural failure of a fuel line will result in a leakage, with the ejected fuel posing a hazard of hot surface ignition (HSI). Under conditions where the fuel line is at high pressure and the localized failure is small, the ejected fuel will form a spray, resulting in a secondary gas flow. A source of difficulty in the analysis of such situations is that the leakage is accidental, introducing a wide range of variability in the operating and boundary conditions. Therefore, safety certification of the associated ignition hazard is supported by an improved understanding of the parametric dependencies of the interaction and ignition of a multiphase flow of fuel spray and air with a hot surface.

By compiling experimental data from numerous studies, Colwell and Reza [1] proposed a qualitative regime diagram for the ignition of liquid fuels, shown in Fig. 1 for $T_w > T_{sat}$, where T_{sat} is the fuel saturation temperature and T_w is the temperature of the hot surface for HSI and the vessel temperature for autoignition. The vertical axis denotes the fuel mass fraction resulting from the total fuel injected into the system. The regime in which HSI occurs is bounded by the dotted line denoted "HSI limit." The authors suggest that the ignition limits are determined by the 'ideality' of the conditions, up to a practically-achievable limit for autoignition denoted by the dashed line labeled "AI limit", beyond which only forced ignition is possible. The minimum achievable autoignition temperature is standardized in the ASTM E 659 test [2], and is denoted T_{AI}. This test is considered to create 'ideal' conditions for ignition by maintaining homogeneous and isothermal conditions on the walls of a cavity containing a flammable mixture under quiescent conditions with a residence time of ten minutes. HSI presents a departure from these conditions through the presence of an evaporating spray, fluid strain, finite residence time and wall heat transfer [3]. Large-scale experiments by Ulcay et al. [4] and experiments by Johnson et al. [5] in a representative section of a military aircraft found a strong dependence of the minimum surface temperature resulting in HSI on the air flow velocity, in agreement with the aforementioned notion of 'ideality'. Quan-

* Corresponding author.
E-mail address: danmohad@stanford.edu (D. Mohaddes).

https://doi.org/10.1016/j.combustflame.2022.111988
0010-2180/

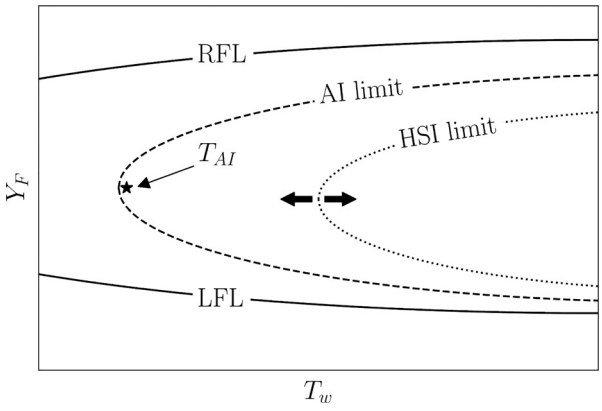

Fig. 1. Qualitative regime diagram for the ignition of liquid fuels, re-created from Colwell and Reza [1] for $T_w > T_{sat}$. The fuel-rich and fuel-lean flammability limits (RFL and LFL, respectively) bound the forced-ignition regime, where ignition is only possible through a localized external energy source, from the non-igniting regime. The dashed line denoted "AI limit" indicates the practically-achievable limit for autoignition standardized by ASTM E 659. The dotted line denoted "HSI limit" indicates the ignition limit for HSI, which varies depending on the conditions considered.

tification of how 'ideal' the conditions are for HSI by determining the parametric dependencies of the ignition limit is an important goal of this study.

The fundamental aspects of HSI have been examined through theoretical and numerical studies of a stagnation-point system. Law [6] employed a matched asymptotic analysis of the steady-state one-dimensional gas-phase boundary-layer equations for a premixed stagnation flow assuming an inner diffusive-reactive zone and an outer diffusive-convective zone. The study arrived at an ignition criterion which can be written in approximate form as $\frac{A}{a}\exp(-T_a/T_w) > 1$, where T_a is the activation temperature, a is the global strain rate and A is the pre-exponential factor of the global reaction. This criterion identifies a clear competition between the effect of the wall temperature through the heat flux into the fluid and the fluid-dynamical strain. Recently, Kats and Greenberg [7], 8] developed an ignition criterion for a two-phase stagnating flow by performing an analysis similar to that of Law [6], but included an Eulerian representation of a dilute fuel spray in their formulation. Their formulation relies upon one-step chemistry and a number of assumptions regarding spray evaporation to make the problem analytically tractable. They arrived at an ignition criterion which can be written in approximate form as $\frac{AC^n}{a^{n+1}}\exp(-T_a/T_w) > 1$, where C is a characteristic evaporation rate and $n > 0$. This criterion reveals that in addition to the competing effects of wall temperature and strain in gas-phase flows, the ignition of a multiphase flow is promoted by an increased rate of spray evaporation.

Numerical work by Aggarwal and Sirignano [9], 10] and Aggarwal [11] focused on the case of a quiescent mixture of n-decane droplets and air in a one-dimensional domain exposed on one side to a hot surface. They employed an Eulerian-Lagrangian approach with one-step chemistry to model the multiphase system. These studies demonstrated that in addition to T_w, the overall equivalence ratio $\phi_0 = Z_{l,0}/f_{st}$, where Z_l is the liquid-to-gas mass ratio and f_{st} is the stoichiometric fuel-air mass ratio, plays a key role in determining the ignition delay time. They also showed that the ignition delay is sensitive to the initial droplet diameter d_0, but showed little sensitivity to the initial gas temperature. Critically, they found that ignition behavior was both quantitatively and qualitatively sensitive to the chemical mechanism employed. Lee et al. [12] considered the steady-state one-dimensional equations to analyze the HSI of dimethyl ether/oxygen cool flames, and demonstrated that the minimum hot surface temperature for cool flame ignition is strongly sensitive to catalytic surface reactions. Recently, large-eddy simulations of a three-dimensional configuration were performed [13] considering a wall-impinging polydisperse n-dodecane/air spray in an Eulerian-Lagrangian formulation using realistic chemistry. This study demonstrated that for wall temperatures near the minimum HSI temperature, a low-temperature ignition significantly preceded high-temperature ignition and subsequent rapid flame propagation throughout the domain. At higher wall temperatures, the ignition delay was greatly reduced, resulting in a diminished extent of flame propagation and a rapid transition to a spatially compact steady-burning flame. In this work, we will employ numerical simulations to consider the effects on ignition of key parameters identified systematically from the governing equations varied across broad ranges.

A key consideration in the analysis of ignition phenomena is precisely how ignition is defined. A common choice [6,14] is the adiabaticity or 'van't Hoff' criterion, $(\partial T/\partial x)_w = 0$. This criterion defines ignition as the condition where the temperature rise in the fluid due to reaction is sufficient such that there is no heat flux into the fluid from the hot surface. This criterion was shown [6] to be equivalent to the 'S'-curve or Semenov-Frank-Kamenetski [15] criterion to leading order. The van't Hoff criterion is amenable to ignition studies that employ continuation methods of the steady-state equations, since it does not require temporal information. Criteria based on the domain-maximum temperature $T_{\max}$ have also been considered, where $T_{\max}$ exceeding a certain temperature threshold in a given configuration is known to result in achieving a fully burning state [16]. If temporal information is available, a possible ignition criterion [17] is that of thermal runaway based on the inflection point in the temporal development of the largest temperature in the domain. It is important to note that the steady-state equations provide information regarding the existence of solutions, but not immediately of their stability [8,18]. Specifically, it has been demonstrated in studies of gas-phase stagnating flames [19] and counterflow spray flames [20,21] that multiple burning solutions can exist for a given set of boundary conditions, and the solution of the steady-state equations does not indicate which of the solutions will be attained for a given set of initial conditions. This information can be obtained from the solution of the unsteady equations given a set of initial and boundary conditions. We take this approach in the present study in order to demonstrate unambiguously the effect of parameter variations on ignition behavior.

Theoretical developments for HSI of impinging sprays have yielded important insights regarding some key parameters, but necessitate significant simplifications to maintain tractable solutions, in particular with regard to chemistry and spray evaporation. Their reliance on a quasi-steady framework as an indicator of ignition precludes any prediction of ignition delay or unsteady dynamics. Steady-state one-dimensional numerical simulations employing realistic chemistry have similar shortcomings. Full three-dimensional simulations provide more detailed descriptions of system dynamics, but their use for the evaluation of the broad parameter space is prohibitively computationally expensive. Therefore, in this work we perform a series of simulations employing an unsteady one-dimensional formulation with realistic models for chemistry and spray evaporation. We do so to achieve sufficient physical fidelity to ensure that the unsteady system dynamics are well-described, while maintaining adequate computational tractability to allow for a broad parametric study. With this approach, we are able to examine the parametric dependencies of the ignition phenomenon and quantify the aforementioned notion of 'ideality' in HSI. To the best of our knowledge, this is the first time this approach has been used to study HSI of a wall-impinging fuel spray.

The remainder of this manuscript is structured as follows. The governing equations and details of the finite-rate chemistry

model employed are presented in Section 2. The physical configuration and parametrization considered in this work is described in Section 3. Unsteady simulation results are first considered in space and time to describe the phenomenology leading to HSI and subsequent flaming in Section 4.1, and effects of problem parameters on ignition behavior are then examined systematically in Section 4.3. Comparisons of the parametric results to a theoretical ignition criterion are discussed in Section 4.4, and the manuscript closes with conclusions in Section 5.

2. Methodology

2.1. Governing equations

We consider the unsteady Navier-Stokes equations for chemically reacting flows in axisymmetric cylindrical coordinates along the $(x, r = 0)$ axis with the conventional assumptions for stagnation flows [22–24], namely that the temperature, mass fractions, axial velocity and the radial velocity gradient vary only in the axial direction. The equations are augmented by solving an energy equation in the solid phase to consider inter-phase heat transfer. Throughout the rest of this manuscript, we will use asterisks to denote dimensional quantities.

The configuration considered is that of a wall-stagnating multiphase flow, shown in Fig. 2. We define the following quantities: radial, axial and time coordinates r^*, x^* and t^*; gas-phase density ρ^*, axial velocity u^*, radial velocity v^*, scaled radial velocity $V^* = v^*/r^*$, temperature T^*, dynamic viscosity μ^*, thermal conductivity λ^*, mixture-averaged diffusivity of the kth species $\mathcal{D}_k^*$, isobaric heat capacity c_p^*, reaction rate of the kth species $\dot{\omega}_k^*$, pressure p^* and scaled radial pressure gradient $\Lambda^* = (\partial_r p^*)/r^*$; droplet mass m_d^*, spray-phase axial velocity u_d^*, radial velocity v_d^*, scaled radial velocity $V_d^* = v_d^*/r^*$, temperature T_d^*, liquid density ρ_l^*, heat capacity c_l^* and droplet relaxation time τ_d^*. These quantities are non-dimensionalized as follows:

$$
\begin{aligned}
&r = \frac{r^*}{\ell^*}, && x = \frac{x^*}{\ell^*}, && t = \frac{t^*}{\tau_f^*}, && \rho = \frac{\rho^*}{\rho_0^*}, && u = \frac{u^*}{\ell^*/\tau_f^*},\\
&v = \frac{v^*}{\ell^*/\tau_f^*}, && V = \frac{V^*}{a^*}, && T = \frac{T^*}{T_0^*}, && \mu = \frac{\mu^*}{\mu_0^*}, && \lambda = \frac{\lambda^*}{\lambda_0^*},\\
&\mathcal{D}_k = \frac{\mathcal{D}_k^*}{\mathcal{D}_0^*}, && c_p = \frac{c_p^*}{c_{p,0}^*}, && \dot{\omega}_k = \frac{\dot{\omega}_k^*}{\dot{\omega}_0^*}, && p = \frac{p^*}{p_0^*}, && \Lambda = \frac{\Lambda^*}{\rho_0^* a^{*2}},\\
&m_d = \frac{m_d^*}{m_{d,0}^*}, && u_d = \frac{u_d^*}{\ell^*/\tau_f^*}, && v_d = \frac{v_d^*}{\ell^*/\tau_f^*}, && V_d = \frac{V_d^*}{a^*}, && T_d = \frac{T_d^*}{T_0^*},\\
&\rho_l = \frac{\rho_l^*}{\rho_{l,0}^*}, && c_l = \frac{c_l^*}{c_{p,0}^*}, && \tau_d = \frac{\tau_d^*}{\tau_{d,0}^*}, &&&&
\end{aligned}
\tag{1}
$$

where the dimensional reference quantities ρ_0^*, u_0^*, T_0^*, μ_0^*, λ_0^*, $c_{p,0}^*$, $\rho_{l,0}^*$ and $m_{d,0}^*$ refer to quantities evaluated at the inlet to the domain of Fig. 2, $\mathcal{D}_0^*$ is the mixture-averaged diffusivity of the fuel vapor at the inlet and p_0^* is the isobaric system pressure. a^* is the global strain rate and $\tau_f^* = 1/a^*$ is the convective time scale. The characteristic length ℓ^* scales with the nominal boundary layer thickness through the strain rate as $\ell^* = (\mu_0^*/\rho_0^* a^*)^{1/2}$ [25]. $\dot{\omega}_0^* = (\dot{\omega}_{CO}^* + \dot{\omega}_{CO_2}^* + \dot{\omega}_{H_2}^* + \dot{\omega}_{H_2O}^*)_0$ is the maximum reaction rate of the progress variable for a stoichiometric free flame with unburned temperature T_0^*. $\tau_{d,0}^* = \frac{\rho_{l,0}^* d_0^{*2}}{18\mu_0^*}$ is the characteristic droplet relaxation time, where the initial droplet diameter d_0^* is evaluated from $m_{d,0}^* = \frac{\pi}{6}\rho_{l,0}^* d_0^{*3}$. Additional reference quantities are the fluid domain length L^*, solid domain thickness L_s^*, solid thermal diffusivity α_s^* and liquid heat of vaporization K_v^*.

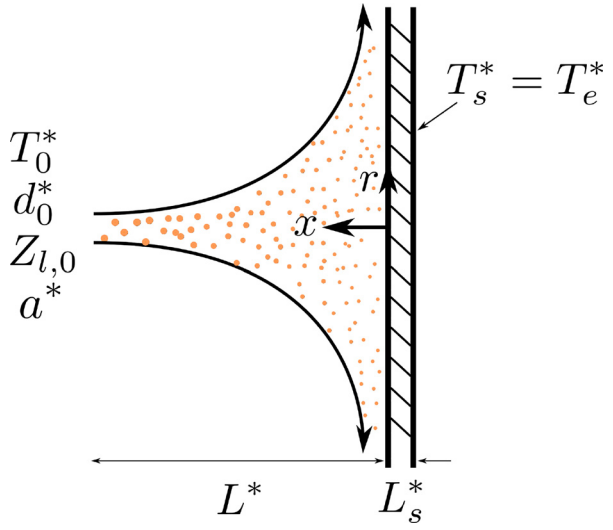

Fig. 2. Physical configuration considered.

Denoting source terms arising from the spray phase as $\dot{S}$, the governing equations in the gas phase are [21,26,27]:

$$\partial_t \rho + 2\rho V + \partial_x(\rho u) = \frac{1}{\mathrm{St}}\dot{S}_\rho, \tag{2a}$$

$$\rho\partial_t V + \rho V^2 + \rho u\partial_x V = \partial_x(\mu\partial_x V) - \Lambda + \frac{1}{\mathrm{St}}\dot{S}_{\rho V}, \tag{2b}$$

$$\rho c_p\partial_t T + \rho c_p u\partial_x T = \frac{1}{\mathrm{Pr}}\partial_x(\lambda\partial_x T) + \mathrm{Da}\dot{\omega}_T + \frac{1}{\mathrm{St}}\dot{S}_{\rho e}, \tag{2c}$$

$$\rho\partial_t Y_k + \rho u\partial_x Y_k = \frac{1}{\mathrm{Sc}}\partial_x(\rho\mathcal{D}_k\partial_x Y_k) + \mathrm{Da}\dot{\omega}_k + \frac{1}{\mathrm{St}}\dot{S}_{\rho Y_k}, \tag{2d}$$

where $\dot{\omega}_T = -\sum_{i=1}^{N_s} h_i\dot{\omega}_i$ is the heat release rate arising from combustion chemistry in the N_s-species chemical mechanism with each species having specific enthalpy h_i, and Y_k is the mass fraction of the kth species. Non-dimensional groups are defined as follows: Stokes number $\mathrm{St} = \tau_{d,0}^*/\tau_f^*$; Prandtl number $\mathrm{Pr} = \mu_0^* c_{p,0}^*/\lambda_0^*$; Schmidt number $\mathrm{Sc} = \mu_0^*/\rho_0^*\mathcal{D}_0^*$; and Damköhler number $\mathrm{Da} = \dot{\omega}_0^*/\rho_0^* a^* = \tau_f^*/\tau_c^*$, where $\tau_c^* = \rho_0^*/\dot{\omega}_0^*$ is the characteristic chemical time scale. In this formulation, the scaled radial pressure gradient Λ is constant in space and the axial momentum equation is not explicitly time-advanced [22]. The ideal gas equation of state is employed.

Considering a multicontiuum (i.e., Eulerian-Eulerian) approach in non-dimensional form Xie et al. [21], a dilute monodisperse spray phase in the same configuration as described above is governed by the equations [21,27]:

$$\partial_t m_d + u_d\partial_x m_d = \frac{1}{\mathrm{St}}\dot{m}_d, \tag{3a}$$

$$\partial_t u_d + u_d\partial_x u_d = \frac{f_1}{\mathrm{St}}\frac{(u - u_d)}{\tau_d}, \tag{3b}$$

$$\partial_t V_d + V_d^2 + u_d\partial_x V_d = \frac{f_1}{\mathrm{St}}\frac{(V - V_d)}{\tau_d}, \tag{3c}$$

$$c_l\partial_t T_d + c_l u_d\partial_x T_d = \frac{1}{\mathrm{St}}\left(\dot{q}_d + \frac{1}{\mathrm{Ja}}\frac{\dot{m}_d}{m_d}\right), \tag{3d}$$

$$\partial_t Z_l + u_d \partial_x Z_l = \frac{1}{\mathrm{St}} Z_l \frac{\dot{m}_d}{m_d}, \tag{3e}$$

$$\dot{m}_d = -\frac{\mathrm{Sh}}{3\mathrm{Sc}} \frac{m_d}{\tau_d} H_M, \tag{3f}$$

$$\dot{q}_d = f_2 \frac{\mathrm{Nu}}{3\mathrm{Pr}} \frac{c_p}{\tau_d} (T - T_d), \tag{3g}$$

where $\dot{m}_d$ and $\dot{q}_d$ are the droplet mass evaporation and heat transfer rates, respectively, with $\dot{m}_d < 0$ indicating mass is lost by the spray and gained by the carrier gas. The non-dimensional groups Nu and Sh are the droplet Nusselt and Sherwood numbers, taken as 2 in this study, and f_1 is the Stokes drag correction [28]. $\mathrm{Ja} = c^*_{p,0} T^*_0 / K^*_\nu$ is the Jakob number. A non-equilibrium Langmuir-Knudsen model (model M7 in [28]) is used to close the evaporative heat transfer correction f_2 and mass transfer potential H_M. This evaporation model is well-validated across a range of droplet and carrier gas temperatures (see the detailed experimental comparisons in [28]) and employs a fully physics-based approach without any arbitrary parameters to capture the transition in evaporation rate as unsaturated droplets reach saturation. An important feature of this model is that it ensures that the droplet temperature does not exceed saturation in the presence of high-temperature gases, which is a key consideration in the case of direct spray-flame interaction as will be considered in Section 4.1.

Source terms coupling the continua are [21,26,27]:

$$\dot{S}_\rho = -n_l \dot{m}_d, \tag{4a}$$

$$\dot{S}_{\rho V} = -n_l \left(\dot{m}_d + \frac{f_1}{\tau_d} m_d \right) (V - V_d), \tag{4b}$$

$$\dot{S}_{\rho e} = -n_l \left(m_d \dot{q}_d - \dot{m}_d \left(c_{p,f} (T - T_d) + \frac{1}{\mathrm{Ja}} \right) \right), \tag{4c}$$

$$\dot{S}_{\rho Y_k} = -n_l \dot{m}_d \delta_{k,F}, \tag{4d}$$

where $c_{p,F}$ is the fuel vapor heat capacity, $n_l = \frac{\rho Z_l}{m_d}$ is the droplet number density, and $\delta_{k,F}$ is the Kronecker delta function, equal to unity when the kth species is identical to the fuel species.

In this study, we consider one-way momentum coupling, and two-way mass and energy coupling between gas and liquid phases. As will be discussed in the following section, we will consider $u = u_d$ and $V = V_d$ at the inlet. We thus approximate $u = u_d$ and $V = V_d$ throughout the governing equations and consequently $\dot{S}_{\rho V} = 0$. The velocity difference arising from spray-gas slip can be approximated to first order as $|u - u_d|/u \sim \mathrm{St}$ [29], and we will thus limit our parametric study to consider $\mathrm{St} \ll 1$ for all simulations. The droplet time scale τ_d remains finite, since droplet diameter (and hence St) is finite at the inlet. Consequently, droplets retain finite thermal inertia and vaporization times. This low-St approximation precludes ambiguities that arise in the modeling of direct spray-wall interactions in an Eulerian-Eulerian formulation by ensuring that the droplets follow the gas-phase streamlines. However, this approximation also has consequences in restricting complex flame structures that have been observed when spray-gas slip is considered, such as double flames [26].

Wall heat transfer is also considered in this study. Heat transfer in the solid phase is modeled by the one-dimensional unsteady energy equation

$$\partial_t T_s = \mathrm{Fo}\, \partial^2_{xx} T_s, \tag{5}$$

where T_s is the solid temperature, $\mathrm{Fo} = \tau^*_f / \tau^*_s$ is the Fourier number and $\tau^*_s = L^{*2}_s / \alpha^*_s$ is the solid-phase thermal diffusion time scale.

2.2. Finite-rate chemistry

The chemical source terms in Eq. (2) are evaluated using finite-rate chemistry by employing a reduced chemical mechanism for n-dodecane/air combustion accounting for both low and high-temperature chemistry [30]. The reduced mechanism has 269 reactions and 54 species, of which 21 are quasi-steady-state (QSS) species identified using a level-of-importance criterion from the original skeletal mechanism [31], which was developed from the USC-II detailed mechanism [32] and thoroughly validated in zero, one and three dimensional settings. The reduced mechanism has been applied previously in simulations of HSI of wall-impinging fuel sprays [13]. Further discussion of the present chemical mechanism and its modeling of low-temperature chemistry is available in [33]. Compared to using a global one-step chemistry approach as has been considered in previous studies [7,8,11], our choice of using a well-validated mechanism derived from detailed chemistry allows for the analysis of minor species in Section 4.1 and lends greater confidence to the quantitative ignition results discussed in Section 4.1, 4.2 and 4.3.

2.3. Numerical methods

The governing equations are time-advanced using the implicit ODE solver CVODE [34]. Coupling is achieved between the solid and fluid phases throughout the course of the unsteady simulations by enforcing the fluid-phase wall heat flux $\dot{q}_w = -(\lambda \partial_x T)_w$ as a Neumann boundary condition in the solid phase, and the solid-phase wall temperature $T_w = (T_s)_w$ as a Dirichlet boundary condition in the fluid phase, as suggested by Radenac et al. [35]. A finite-difference scheme is employed for spatial discretization, with second-order central and first-order upwind stencils employed for the diffusive and convective operators, respectively. Chemical source terms are computed using the open-source combustion chemistry package Cantera [36] customized for use with reduced mechanisms.

3. Physical configuration and parametrization

The configuration considered in this study is motivated by the localized failure of a pressurized fuel line near a hot wall. A leakage flow is ejected from the failure point at a constant pressure and mass flow rate. The leakage flow generates a secondary flow, and the combined flow stagnates axisymmetrically at the hot wall. Depending upon the conditions considered, this configuration can result in the formation of an ignition kernel and subsequent flame propagation. We model this configuration as an unsteady problem in one dimension, as shown in Fig. 2. In the context of the literature, this configuration is most similar to that of Wehrfritz et al. [37], who also considered a wall-impinging n-dodecane flame in a one-dimensional setting, but assumed a fully-premixed gaseous inflow and employed a steady-state formulation motivated by flame-wall interactions in internal combustion engines.

The system under consideration is open to ambient conditions at a pressure of $p^*_0 = 1\,\mathrm{atm}$. The distance between the inlet and the wall is $L^* = 20.0\,\mathrm{mm}$, and we consider strain rates of $a^* = [1, 100]\,\mathrm{s}^{-1}$. We consider the gas and liquid-phase axial velocities at the inlet to the domain to be equilibrated as $u^* = u^*_d$, where $u^*_0 = a^* L^*$, and without radial inflow velocity gradients $V^* = V^*_d = 0\,\mathrm{s}^{-1}$. The liquid-phase mass flow rate can be parametrized by the inflow liquid-to-gas mass ratio $Z_l = Z_{l,0} = [0.03, 0.77]$. We take the gas and liquid-phase inflow temperatures equal to that of the fuel line, $T^* = T^*_d = T^*_0 = 400$ K. We model the leakage flow as a monodisperse n-dodecane spray with an inflow diameter of $d^* = d^*_0 = [8, 346]\mu\mathrm{m}$. We limit the scope of our study to n-dodecane/air combustion as it is a relevant neat surrogate for

Table 1
Summary of dimensional reference quantities constrained by the physical configuration considered.

L^* [mm]	T_0^* [K]	p^* [atm]	ρ_0^* [kg/m^3]	μ_0^* [Pa·s]	$c_{p,0}^*$ [kJ/(kg·K)]	λ_0^* [W/(m·K)]
20.0	400	1.0	0.878	2.30×10^{-5}	1.02	3.29×10^{-2}

$\mathcal{D}_0^*$ [m^2/s]	$\dot{\omega}_0^*$ [kg/(m^3·s)]	f_{st} [−]	$\rho_{l,0}^*$ [kg/m^3]	K_v^* [kJ/K]	L_s^* [mm]	α_s^* [m^2/s]
8.66×10^{-6}	773.0	0.0671	669.4	256.2	3.0	3.8×10^{-6}

safety applications in diverse industries handling jet, diesel and other kerosene-based fuels. For n-dodecane/air combustion, $f_{st} = 0.0671$. At these inflow conditions, liquid n-dodecane has density $\rho_{l,0}^* = 669.4\,\mathrm{kg/m^3}$ and heat of vaporization $K_v^* = 256.2\,\mathrm{kJ/K}$. The hot wall has a thickness $L_s^* = 3\,\mathrm{mm}$ and constant material properties corresponding to stainless steel, with thermal diffusivity $\alpha_s^* = 3.8 \times 10^{-6}\,\mathrm{m^2/s}$, with isothermal exterior wall temperature $T_s^* = T_e^* = [1100, 1300]\,\mathrm{K}$. The domain between the fuel line and the hot wall consists initially of quiescent air with a linear temperature profile between the fuel line temperature T_0^* and the interior wall temperature T_w^*, and between the wall interior and wall exterior at T_e^*, with the interface temperature T_w^* computed dynamically as noted in Section 2.1. The reference properties $\rho_0^* = 0.878\,\mathrm{kg/m^3}$, $\mu_0^* = 2.30 \times 10^{-5}\,\mathrm{Pa{\cdot}s}$, $c_{p,0}^* = 1.02\,\mathrm{kJ/(kg{\cdot}K)}$, $\lambda_0^* = 3.29 \times 10^{-2}\,\mathrm{W/(m{\cdot}K)}$, $\mathcal{D}_0^* = 8.66 \times 10^{-6}\,\mathrm{m^2/s}$ are computed using the properties of air at temperature T_0^* and pressure p_0^*, and $\dot{\omega}_0^* = 773.0\,\mathrm{kg/(m^3{\cdot}s)}$ using the definition given in Section 2.1. The reference quantities constrained by the configuration considered are summarized in Table 1.

The following non-dimensional groups present in the governing equations of Section 2.1 are readily evaluated from the reference quantities: $\mathrm{Pr} = 0.72$, $\mathrm{Sc} = 3.03$, and $\mathrm{Ja} = 1.60$. The ranges specified for d_0^*, a^*, T_e^* and $Z_{l,0}$ result in the following ranges for the non-dimensional quantities to be considered parametrically in this study: $T_e = [2.75, 3.25]$, $\phi_0 = [0.5, 11.5]$, $\mathrm{St} = [0.001, 0.3]$ and $\mathrm{Da} = [9, 900]$. Given the constraints considered, $\mathrm{Fo} \sim \mathrm{Da}$ and is thus not treated as an independent parameter of the problem. Since our study is motivated by safety applications, we seek to consider broad ranges for the above-identified quantities as they are not known *a-priori* in the context of the failure of a pressurized fuel line. Hence, we consider St and Da over two orders of magnitude, as well as a range of fuel-lean and fuel-rich conditions. The Eulerian-Eulerian formulation employed in this study assumes a small liquid mass fraction $\alpha_l < 10^{-3}$. Since the liquid mass fraction is expected to be maximum at the inlet, it follows that this limits the total inflow equivalence ratio to $\phi_0 < \alpha_l \frac{\rho_l}{\rho} \frac{1}{f_{st}} \approx 11.5$. Given that our focus is on ignition, we limit our study to T_e^* above the empirical minimum for HSI of liquid n-dodecane of approximately 950 K [13]. Considering heat transfer within the solid phase, $\mathrm{Fo} = [0.004, 0.4]$ for the range of Da considered in this study. Temperature changes within the solid are thus expected to be negligible over multiple convective time scales, i.e., $T_w \approx T_e$ for time scales relevant to ignition. Heat transfer within the solid phase is retained in the formulation for generality.

4. Results

4.1. Ignition phenomenology

Prior to performing a parametric study, we consider a single case in order to describe the ignition phenomenology and demonstrate the variables we will use in the parametric analysis. The case considered has the following parameter values: $T_e = 3.25$, $\phi_0 = 1.0$, $\mathrm{St} = 0.1$ and $\mathrm{Da} = 124$. As noted in Section 1, a number of ignition criteria have been considered by other authors. In the present configuration, it is possible that initial exothermicity due to a low-temperature ignition is quenched without leading to a high-temperature ignition and subsequent flaming. To distinguish between low and high-temperature ignition and focus on the latter because of its greater relevance to safety, we apply a temperature threshold criterion [13]. We have found this to be more reliable than other criteria. We define the time and location of ignition as:

$$t_{ign} = \mathrm{argmin}_t \left| \max_x(\theta) - \theta_{ign} \right|, \tag{6a}$$

$$x_{ign} = \mathrm{argmin}_x \left| \theta(x, t_{ign}) - \theta_{ign} \right|, \tag{6b}$$

where $\theta(x,t) = (T-1)/(T_{ad}-1)$ and $T_{ad} = 5.82$ is the adiabatic flame temperature evaluated for a stoichiometric mixture at $T = 1$. θ_{ign} was taken as 0.6 based on a sensitivity analysis of the ignition results for the configuration considered in this study. Using this criterion, ignition occurs at $x_{ign} = 1.26$ and $t_{ign} = 1.89$ for the case considered in this section. The time and location of ignition are shown by a star in Fig. 3. In this case, $1/\mathrm{Fo} = 16.9 \gg t_{ign}$, and hence the wall is effectively isothermal with $T_w \approx T_e$ for time scales relevant to ignition and flame propagation.

The development of the fluid dynamical structure is shown in Fig. 3a using the scaled radial velocity V. Beginning with initially quiescent conditions, the flow moves toward the wall at $x = 0$. A velocity profile is established, with a viscous boundary layer near the wall. In the present non-dimensionalization, the thickness δ of the viscous layer in a stagnation configuration can be approximated as $\delta \approx 2.0$ [25], which is in reasonable agreement with the results seen in the figure. The viscous layer is seen to reach its steady profile by approximately $t = 1$, prior to ignition. A key observation is that ignition occurs within the boundary layer, i.e., $\delta > x_{ign}$. The subsequent flaming results in the rapid reduction of post-flame density and thus an acceleration of the radial flow.

Droplets are transported toward the wall by the gas-phase flow, as seen by the development of the local liquid equivalence ratio $\phi_l = Z_l/f_{st}$ in Fig. 3b. In Fig. 3c showing T_d, areas where $\phi_l < 0.1$ are grayed out, as T_d is not a meaningful quantity where there is no spray. Since spray transport is purely convective, prior to ignition, the carrier gas temperature remains near the inlet temperature $T = 1$. The droplet temperature therefore remains near $T_d = 1$ in most of the domain, with some reduction in droplet temperature due to the latent heat of vaporization. However, at the leading edge of the spray front (shown in the figures as a dashed green line), T_d increases due to heat exchange with the carrier phase. Nevertheless, prior to ignition, droplet temperature remains below saturation in the diffusion-dominated evaporation regime. After ignition, interaction of the spray with the flame away from the wall results in the rapid local increase of T_d to the saturation temperature for n-dodecane of $T_{sat} = 1.22$. Spray evaporation in this region thus increases, resulting in rapid spray consumption, as seen from the post-ignition evolution of ϕ_l in Fig. 3b.

The thermo-chemical evolution of the gas phase is shown in Fig. 3d–g. As discussed in Section 3, the temperature profile in the initially quiescent gas phase is linear between the inlet and the wall. Considering Fig. 3e, this initial temperature profile evolves into a thermal boundary layer due to the stagnating flow. Through

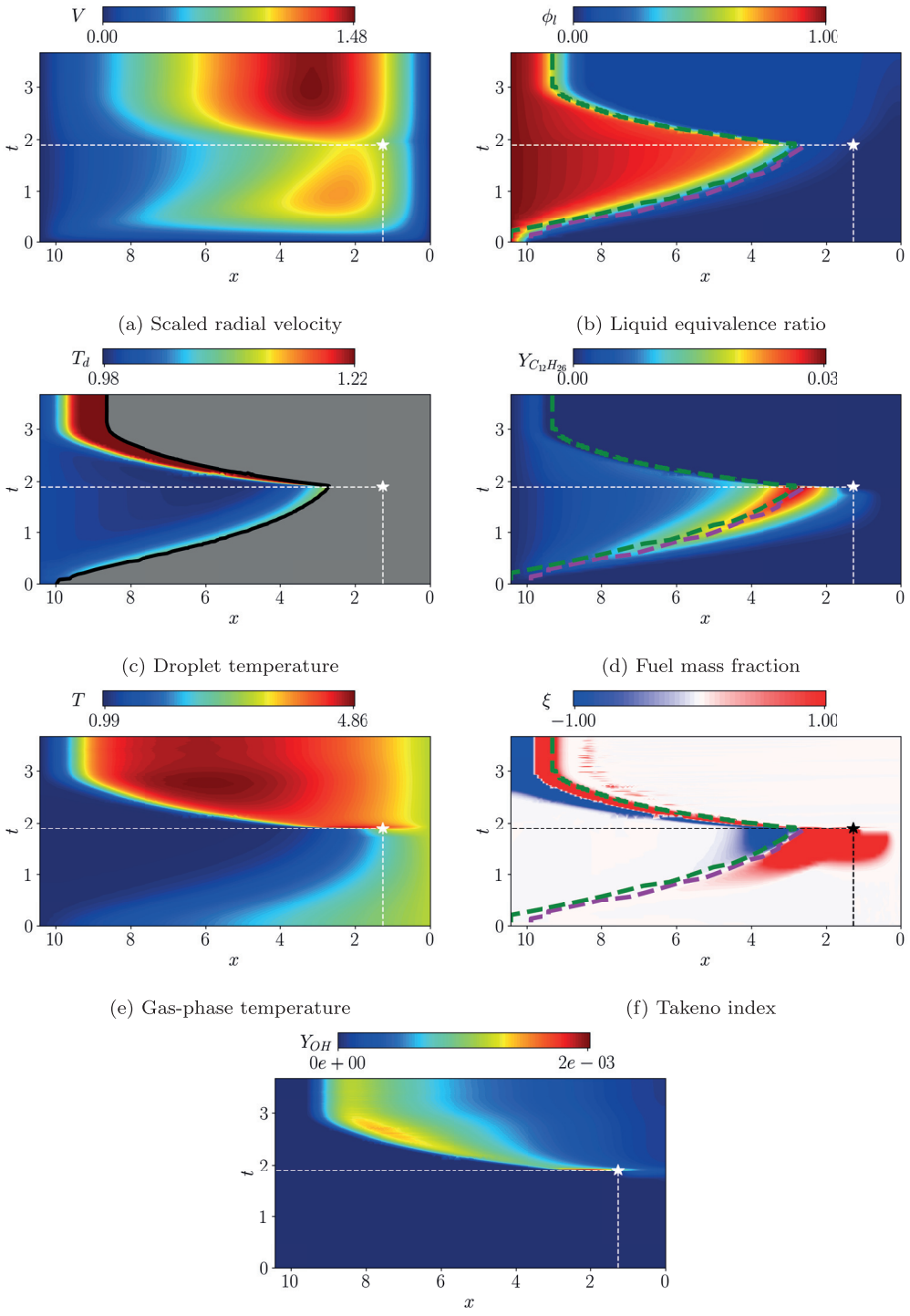

(a) Scaled radial velocity

(b) Liquid equivalence ratio

(c) Droplet temperature

(d) Fuel mass fraction

(e) Gas-phase temperature

(f) Takeno index

(g) OH mass fraction

Fig. 3. HSI of a wall-impinging fuel spray. The intersection of the thin dashed lines at the star indicates the time and location of ignition. The dashed magenta line shows the location of the maximum fuel mass fraction x_F, and the dashed green line shows the spray front. (For interpretation of the references to color in this figure legend, the reader is referred to the web version of this article.)

interaction with the spray phase, the evaporating droplets produce fuel vapor, shown in Fig. 3d. At all times prior to ignition there is a spatial location $x = x_F$ of maximum fuel vapor mass fraction, indicated by the dashed magenta line. Considering again Fig. 3b for the liquid equivalence ratio ϕ_l and comparing it to $Y_{C_{12}H_{26}}$, we see that x_F (dashed magenta line) closely follows the spray front (dashed green line) across time. Although the case is globally stoichiometric, we find that the spray evaporation results in locally lean mixtures, even at x_F. The spray evaporation also causes a local reduction in gas temperature, resulting in a minimum temperature of approximately $T = 0.99$, as has been observed in studies of counterflow spray flames [21].

In considering Fig. 3d, we find that $x_{ign} < x_F(t_{ign}) \approx 2.5$. Defining the gas-phase equivalence ratio at (x_{ign}, t_{ign}) as $\phi_{ign} = \frac{Z}{f_{st}(1-Z)}$,

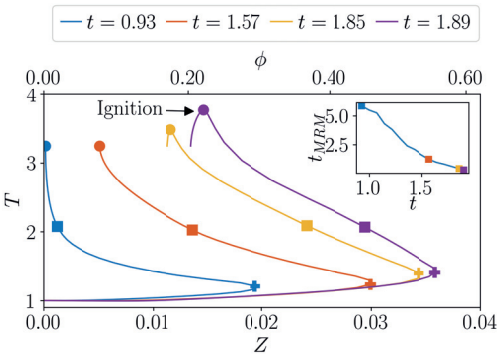

Fig. 4. Unsteady temperature profiles in composition space, with equivalent values of mixture fraction Z and equivalence ratio ϕ shown on the lower and upper horizontal axes, respectively. For each time shown, circles, crosses and squares indicate $(Z|_{\max(T)}, \max(T))$, $(\max(Z), T|_{\max(Z)})$, and $(Z, T)_{MRM}$ respectively. The profile at $t = 1.89$ corresponds to $t = t_{ign}$. The inset figure shows the time-evolution of the ignition delay for the most reactive mixture, t_{MRM}.

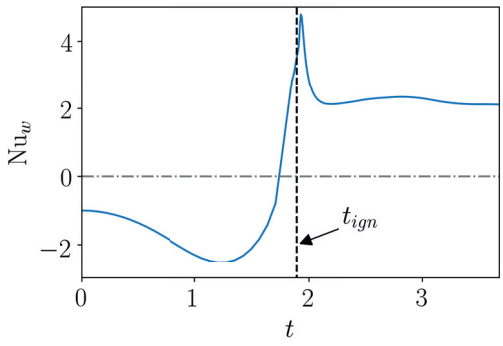

Fig. 5. Wall heat flux Nusselt number Nu_w, where the dashed line shows the time of ignition and the dash-dotted line indicates $\mathrm{Nu}_w = 0$.

where Z is the Bilger mixture fraction [38], we have $\phi_{ign} = 0.22$, whereas at the same time instant the equivalence ratio at x_F is $\phi_F(t_{ign}) = 0.56$. The ignition kernel thus forms nearer to the wall and at a much leaner condition than that of x_F. This can be understood by considering the ignition process in gaseous composition space, shown in Fig. 4. At $t = 0.93$, a full convective time scale has not yet elapsed and the fuel vapor formed by the incoming spray has thus not yet reached the wall. The maximum temperature in the domain occurs at $Z|_{\max(T)} = 0.0$, with $\max(T) = T_w$, since sufficient heat release has not yet occurred to raise the gas temperature beyond T_w. At $t = 1.57$, fuel vapor has reached the wall such that $Z|_{\max(T)} > 0.0$, but the maximum temperature remains T_w. By $t = 1.85$, sufficient heat release has occurred such that $\max(T) > T_w$, and the ignition criterion is met at $t = 1.89$. As has been discussed in the literature in the context of both homogeneous reactors and high-fidelity simulations [39,40], the most reactive mixture composition is a function of the mixture temperature. The most reactive mixture for high-temperature n-dodecane/air mixtures in particular has been shown to be fuel-lean [40]. In the present case, both temperature and composition profiles are developing in time due to the combined effects of convection and spray evaporation, and the most reactive mixture thus varies with time as well. For each instantaneous $Z - T$ profile, we can determine the most reactive mixture present in the domain $(Z, T)_{MRM}$ by considering the minimum homogeneous reactor ignition delay time among all mixtures within the profile, denoted t_{MRM}. $(Z, T)_{MRM}$ and t_{MRM} are shown using square symbols in the unsteady profiles and inset of Fig. 4, respectively. The highest Z in the domain, denoted by the cross symbols for each profile and which correspond to x_F and ϕ_F, occurs at a relatively low temperature compared to T_w in each profile. The most reactive mixture, however, occurs consistently on the 'upper' branch, between $(Z|_{\max(T)}, \max(T))$ and $(\max(Z), T|_{\max(Z)})$. For a given Z, the high-temperature upper branch is consistently more reactive than the lower branch. Since the upper branch corresponds to $x < x_F$ and $\phi < \phi_F$, ignition ultimately occurs nearer to the wall and at fuel-leaner conditions than x_F and ϕ_F. This is a key insight into the phenomenology of HSI of wall-impinging sprays, and will be revisited in the parametric study of Section 4.3.

In Fig. 3f, we employ the Takeno flame index $\xi = \nabla Y_{C_{12}H_{26}} \cdot \nabla Y_{O_2}$ [41] to identify premixed and non-premixed regions, as has been applied in previous studies of spray combustion [42,43]. Positive and negative values of ξ respectively indicate premixed and non-premixed regions, and $\xi \approx 0$ indicates regions with negligible fuel and/or oxidizer gradients. The color map has been saturated to clearly identify the different regions. The figure shows that prior to ignition, the location of maximum fuel mass fraction x_F delineates a transition in the Takeno index, with $x < x_F$ corresponding to a premixed region, whereas $x > x_F$ is non-premixed. As was discussed above, $x_{ign} < x_F$, and thus in the case considered, ignition and initial flame propagation occur in a premixed region.

Of the two flames resulting from ignition, the flame propagating upstream produces fuel vapor through increased spray evaporation due to its interaction with the spray phase, as was shown in Fig. 3b. The upstream flame continues to react exothermically and eventually stabilizes near the inlet, as seen from the OH mass fraction in Fig. 3g. By contrast, the flame propagating toward the wall is exposed to yet fuel-leaner mixtures, with no spray available for evaporation. This flame therefore rapidly quenches on the wall, as seen from the sudden reduction in OH mass fraction near the wall. The system ultimately reaches a steady-state with the flame stabilized near the inlet at $t \approx 3$.

A key consideration for safety analysis is the wall heat flux imparted by an ignition event. We consider wall heat flux through the wall Nusselt number in Fig. 5, computed as

$$\mathrm{Nu}_w = \frac{(\partial_x T)_w}{(T_w - 1)/L}, \tag{7}$$

where $\mathrm{Nu}_w > 0$ indicates heat flux from the fluid into the wall. Initially $\mathrm{Nu}_w = -1$, since the initial temperature profile is linear and the gas phase is initially quiescent, as discussed in Section 3. Convection results in Nu_w becoming more negative. As ignition is approached, Nu_w changes sign, as seen from the blue line crossing the dash-dotted gray line at $\mathrm{Nu}_w = 0$. Shortly after ignition at t_{ign}, shown by the dashed black line, Nu_w reaches a maximum as the downstream-propagating flame quenches on the wall in the manner discussed above. Similar temporal variation in wall heat flux after HSI was demonstrated in high-fidelity simulations [13]. Here, we can clearly identify the wall heat flux behavior as resulting from head-on quenching [44]. As was shown above, the region $0 < x < x_F$ is identified as premixed using the flame index, and furthermore it was found that $x_{ign} < x_F$. We thus conclude that the wall-impinging fuel spray results in the formation of a region of premixed fuel vapor inside the thermal boundary layer corresponding to the most reactive mixture in the domain. The ensuing ignition in this region produces two flames, the downstream-propagating of which quenches on the wall, producing a peak in the wall heat flux. Nu_w subsequently remains positive as the high temperature combustion products generated by the upstream flame are convected toward the wall.

4.2. Parameter importance ranking

The key interest of this work is in analyzing the parametric dependencies of ignition behavior, and furthermore in verifying and

quantifying the parameters identified empirically in Section 1 as critical in controlling HSI. We proceed by quantifying the parametric dependencies of the HSI event on the system parameters identified in Section 3 in order to identify the most important relationships. We do so by employing a data analysis method, namely the permutation importances of random forest classifiers/regressors [45]. Random forests have recently been applied successfully to problems in data-assisted combustion modeling [46] and other applications. Here, we consider random forests due to their interpretability when considered in the context of permutation importances. This involves the training of a random forest model for each output variable and then considering the change in model score caused by the shuffling (i.e. permutation) of feature values in the test set. The mean permutation importance of a feature for a particular output variable is the average decrease in model score when that feature is randomly shuffled. The relative magnitude of the mean permutation importance is thus a measure of the importance of a given feature in determining the output, allowing the features to be ranked in order of importance for each output, so long as the features are statistically independent. We consider the system parameters T_e, ϕ_0, log(St) and log(Da) in the ranges noted in Section 3 as *features*, and simulation results for t_{ign}, ϕ_{ign} and x_{ign} as well as whether ignition occurred as *outputs*, with the latter output a Boolean value to be *classified*, and all others real valued quantities to be *regressed*. We define the ignition limit to be the boundary of a Boolean variable in parametric space between parameter values resulting in ignition, i.e. 'igniting', and those that do not, i.e. 'non-igniting'. In each simulation, the same criterion discussed in Section 4.1 is used to identify ignition. A case was determined to be non-igniting if it did not achieve the ignition criterion by $t^* = 3.0\,\mathrm{s}$, which was 30% larger than the largest t^*_{ign} observed in this study. A dimensional criterion was used to ensure consistency across simulations, since non-dimensional time is affected by a given case's parameters through the inflow velocity. The features are independent by construction, as per the problem parametrization of Section 3. The use of the logarithms of St and Da results in an improvement in model accuracy by reducing data sparsity since these parameters vary across two orders of magnitude, but the feature importance rankings were found to be robust to this choice. The model score is evaluated for classification using model accuracy, i.e., the fraction of correct predictions, and for regression using the coefficient of determination. Since the coefficient of determination can be negative, permutation importances can be greater than unity for regressors.

Prior to evaluating the relative feature importances, random forests were trained and tested to ensure their predictive accuracy. The ignition feature classifier was trained and tested on the full data set of 925 simulations, and the regressors for t_{ign}, ϕ_{ign} and x_{ign} were trained and tested on the igniting subset of 444 simulations. We employed an 80%/20% split between training and test data for all outputs and considered random forests with 100 trees. Training set accuracy for all random forests was greater than 95%, and test set accuracy was greater than 90%.

The results of the permutation importance analysis of the ignition classifier are shown as a box-and-whiskers plot in Fig. 6. Since we are interested in the most important parametric relationships, we rank the features in order of importance using the mean permutation importance values, shown as dashed black lines in the figure. However, the figure shows that there is substantial variation about the mean value. This is a consequence of the non-linearity of the problem considered, in that the quantitative effect of a given parameter on an output variable is dependent on the value of that and all other parameters, thus yielding a range of permutation importances. The feature importance rankings resulting from the permutation importance analysis of all output variables are summarized in Table 2. The rankings are based on the mean permutation

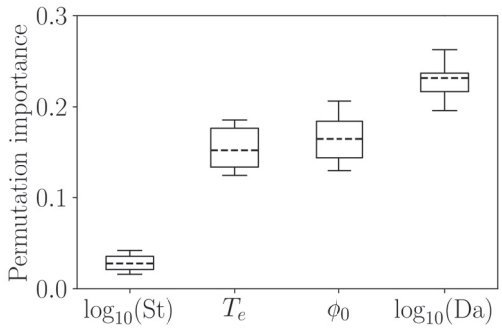

Fig. 6. Permutation importances for the ignition classifier, with mean values shown by the dashed black lines.

Table 2
Feature importance rankings for all output variables considered. Mean permutation importances are shown in parentheses, indicative of the change in model accuracy for an output variable when a given feature is shuffled.

	$\log_{10}(\mathrm{Da})$	$\log_{10}(\mathrm{St})$	T_e	ϕ_0
Ignition	1 (0.23)	4 (0.03)	3 (0.15)	2 (0.16)
t_{ign}	1 (1.15)	4 (0.09)	3 (0.17)	2 (0.51)
x_{ign}	1 (1.60)	4 (0.01)	2 (0.73)	3 (0.04)
ϕ_{ign}	2 (0.85)	4 ($< 10^{-3}$)	1 (1.45)	3 (0.30)

importance values, which are also provided. Although the rankings were found to be robust to statistical variation emanating from the random selection of the training and test sets, the mean permutation importance values themselves exhibit some variation due to the smallness (by machine learning standards) of the data set used. For t_{ign}, x_{ign} and ignition classification, Da is found to be the most important parameter, substantially so for the former two quantities. By contrast, St is ranked last for all outputs and only has a significant effect on t_{ign} and ignition classification, with almost no effect on x_{ign} and ϕ_{ign}. A greater importance would be expected for St if droplets were not prescribed to follow gas-phase streamlines, as noted in Section 2.1, since the present formulation precludes complex behaviors associated with spray-gas slip observed in counterflow configurations [26,47]. Although ϕ_0 is ranked second or third for all outputs, it has little quantitative effect on x_{ign} when its mean permutation importance is compared to those for Da and T_e. We also see that unlike all other outputs, the most important parameter determining ϕ_{ign} is by far T_e, followed by Da, with ϕ_0 having little quantitative importance.

The parameter importance rankings indicate the leading relationships present in the highly-coupled non-linear system in a quantitative and statistically robust manner for the parameter ranges considered. Motivated by the observed parameter importances, the following section considers a number of relationships between system parameters and ignition behavior through physical analysis.

4.3. Parametric analysis

As was noted in Section 1, previous experimental studies have investigated parametric dependencies and 'idealness' of HSI behavior for wall-impinging sprays, but did not do so systematically in the present canonical configuration. Theoretical studies [7,8] have indeed considered the parametric dependencies systematically, but were limited to qualitative analyses due to the assumptions required for analytical tractability, and focused only on the ignition limit due to the quasi-steady formulation employed. Here, we consider the effects of the independent non-dimensional parameters identified in Section 3 on the ignition limit, as well as the time, location and local composition of ignition using unsteady numerical

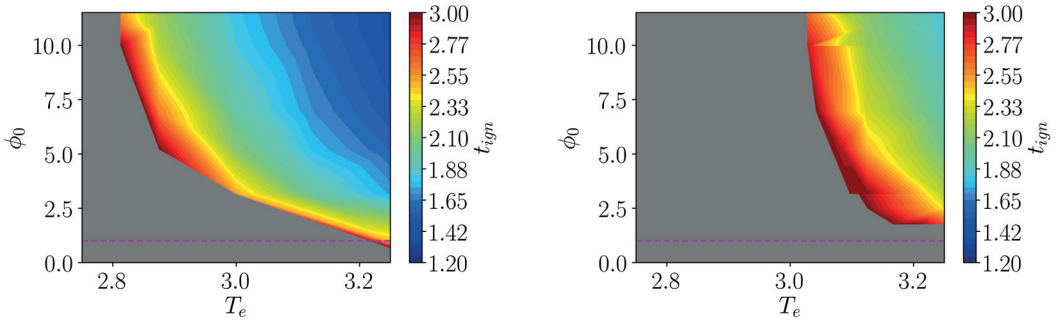

(a) Ignition delay, t_{ign}

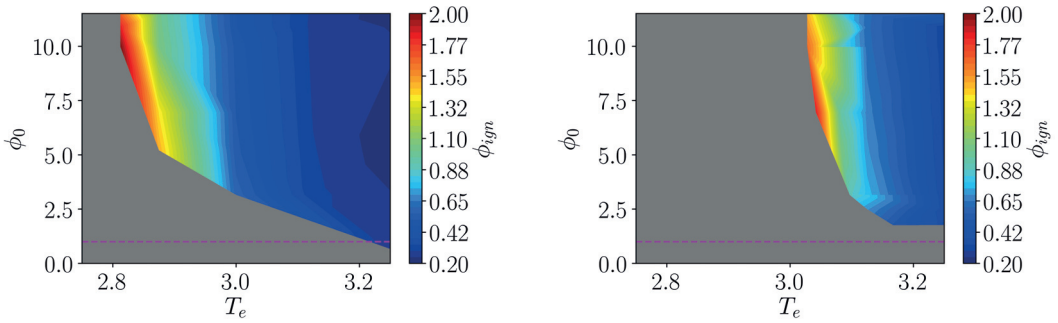

(b) Equivalence ratio at ignition, ϕ_{ign}

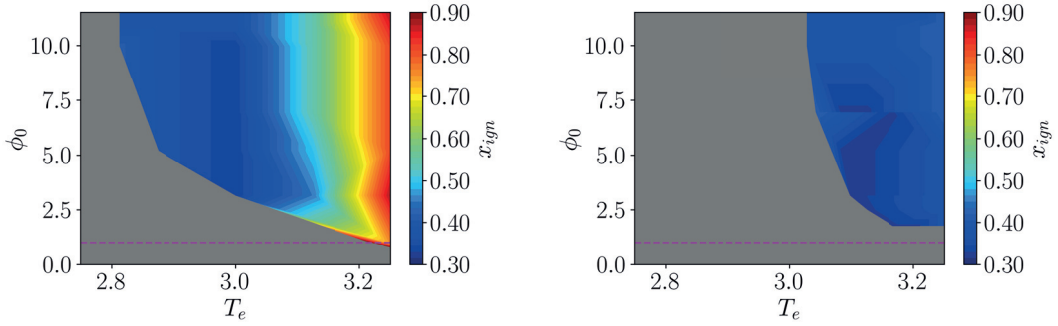

(c) Ignition location, x_{ign}

Fig. 7. Parametric ignition results for St = 0.1. Left column: Da = 70, right column: Da = 35. Gray indicates non-igniting conditions, and the dashed magenta line indicates $\phi_0 = 1$.

simulations. We do so in order to analyze parametric dependencies and to quantify the notion of 'ideality' of conditions for HSI.

We consider first the results for constant St in Fig. 7, with the left column showing results for Da = 70 and the right for Da = 35. In all panels, the extent of the colored contours indicates the ignition limit, with the gray areas not resulting in ignition. By comparing the results for the different Damköhler numbers, we see that the reduction of Da by a factor of two results in a significant contraction of the ignition limit toward high temperatures and fuel-rich inflow conditions. At Da = 35, ignition is only achieved at $T_e > 3.0$, even for the richest ϕ_0 considered. Fuel-lean and near-stoichiometric inflow conditions also become non-igniting, with a minimum ϕ_0 for ignition of approximately 1.8. This behavior is in close agreement with the qualitative regime diagram for HSI of liquid fuels of Colwell and Reza [1] shown in Fig. 1. Across all igniting simulations considered in this study, $|T_w - T_e| < 0.01$. Thus, for the purpose of comparison to the figure, $T_w \approx T_e$, as expected from the discussion in Section 3.

Figure 1 shows that less 'ideal' conditions result in the limit for HSI shifting to fuel-richer conditions and higher surface temperatures, with increasingly less 'ideal' conditions yielding a more restricted regime of parameters resulting in HSI. In Fig. 7, we have demonstrated this phenomenon through simulations for $\phi_0 < 11.5$. The key parameter for quantifying the notion of 'idealness' of conditions for HSI at a given ϕ_0 and T_e is thus Da, as is supported by the permutation importance rankings for the ignition limit in Table 2, where Da was shown to be the most important parameter in determining ignition. This is supported by the ignition literature for counterflow flames, where it is well-established that for constant thermo-chemical conditions in the inflow streams, the strain rate (parametrized here by Da) is the key parameter determining the boundary between autoignition and extinction (e.g., [48,49]) and influencing the development of the ignition kernel [50]. The present configuration has a further parameter, St, whose effect on ignition and 'idealness' will be discussed in the context of Fig. 8 below.

The parametric variation of t_{ign} is demonstrated in Fig. 7a. For both Da considered, t_{ign} is shortest at high T_e, as expected on basic thermo-chemical grounds, but also at highly fuel-rich conditions. The ignition delay increases rapidly as the ignition limit is

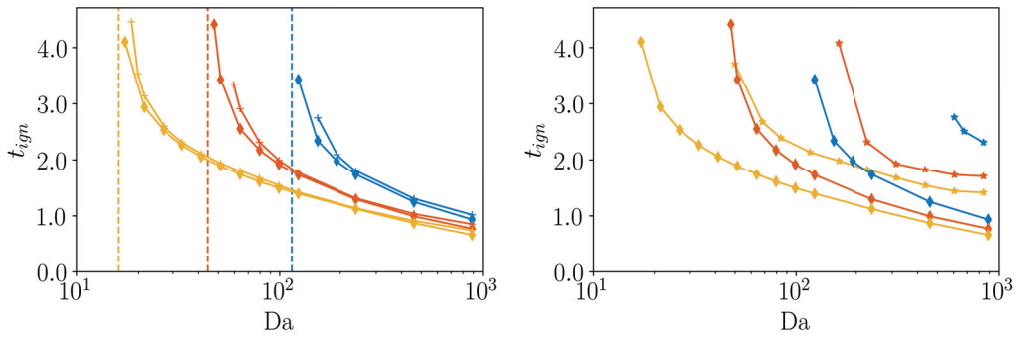

(a) Ignition delay, t_{ign}. Dashed lines in left panel show ignition limit for St = 0.01

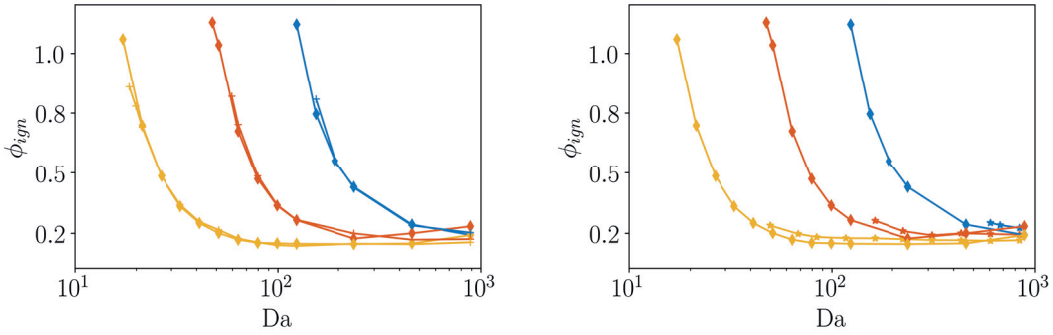

(b) Equivalence ratio at ignition, ϕ_{ign}

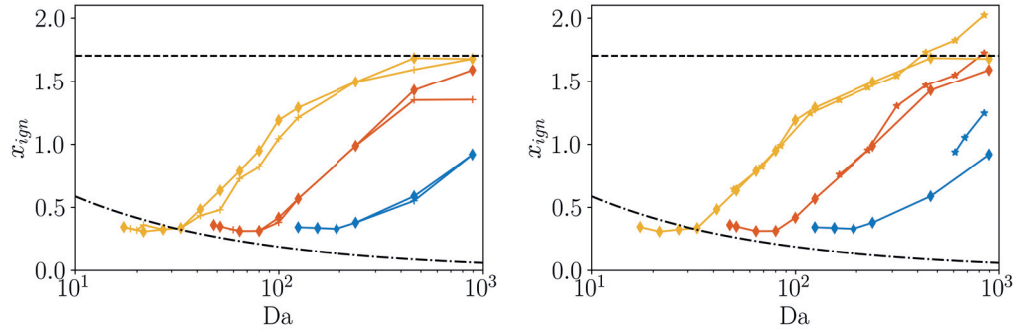

(c) Ignition location, x_{ign}. Dashed black line indicates δ_T, and dash-dotted black line δ_F.

Fig. 8. Parametric ignition results. Left column: ignition results for $\phi_0 = 3.0$; St = 0.01 (♦), St = 0.1 (+). Right column: Ignition results for St = 0.01; $\phi_0 = 0.7$ (⋆), $\phi_0 = 3.0$ (♦). $T_e = 2.75$ ——, $T_e = 3.0$ ——, $T_e = 3.25$ ——.

approached, as is also the case in autoigniting counterflow flames [49]. It is noteworthy that, although the homogeneous reactor ignition delay time varies by more than an order of magnitude across the temperature range considered [13], the HSI delay time varies by less than a factor of three at constant Da. Furthermore, the decrease in t_{ign} with increasing ϕ_0 cannot be immediately explained from the reduction in homogeneous reactor ignition delay time, as the ignition kernel does not form at the same composition as the inlet. In fact, from Fig. 7b, it is evident that the inlet composition has little effect on the ignition kernel composition, being determined by T_e and Da. Similarly, at Da = 70 the location of ignition kernel formation is found to be insensitive to ϕ_0 and is determined primarily by T_e, as confirmed by the permutation importance rankings of Table 2. At constant Da and ϕ_0, the dependence on T_e can be understood by considering the role of the thermal boundary layer on the ignition process, as noted in Section 4.1. Absent any heat release and at a constant Da (and thus a constant strain rate), at higher T_e the highest fluid temperatures will extend further away from the wall. It would thus be expected that ignition would also occur at an increased distance from the wall, since we are using a temperature-based ignition criterion. In Section 4.1 we noted that in the present non-dimensional formulation, the boundary-layer thickness is approximately constant at $\delta \approx 2.0$, and is thus not expected to vary with Da. However, at Da = 35 and plotting on the same color scale, it is evident that for constant T_e and ϕ_0, x_{ign} is substantially reduced relative to the higher Da results. We will discuss this in greater detail in the context of Fig. 8c. The relative variation in x_{ign} at the lower Da condition is also diminished, with a difference between the maximum and minimum values for x_{ign} in the Da = 35 panel of Fig. 7c of only approximately 20%, whereas the variation in the Da = 70 panel is greater than a factor of two.

In Fig. 8 we plot results from a limited number of simulations that resulted in ignition in parametric ranges that are illustrative of some of the effects discussed above. The sensitivity of t_{ign} to ϕ_0 is seen in the right panel of Fig. 8a. A reduction of ϕ_0 from 3.0 to 0.7 is seen to result in an increase in t_{ign} by approximately a factor of two, as well as a contraction of the ignition limit toward larger Da, as was also demonstrated in Fig. 7. The left panel of Fig. 8a

clearly shows the increase in t_{ign} with decreasing Da as the ignition limit is approached. Similar behavior was observed and discussed in the context of Fig. 7a when the ignition limit was approached at constant Da through variation in ϕ_0 and T_e. The effect of St on t_{ign} and on the ignition limit can be seen from the left panel of Fig. 8a. Larger values of St result in a contraction of the ignition limit to larger Da, and moderately larger t_{ign} near the ignition limit. Of note, however, is that the order of magnitude variation in St results in virtually no change in t_{ign} at higher Da away from the ignition limit. In the present formulation which assumes droplets follow gas-phase streamlines, ignition behavior has low sensitivity to initial droplet diameter. Variation in St is found to be primarily of importance at low Da near the ignition limit. In particular, an increased value of St results in less 'ideal' conditions for HSI in the context of Fig. 1, though its effect is quantitatively less important than that of Da, as shown in Table 2. Consideration of spray-gas slip would likely increase the importance of St for HSI and lead to more complex behavior, as discussed in Sections 2.1, 4.2.

If the processes leading to HSI of the impinging fuel sprays considered were linearly coupled, then t_{ign} could be estimated as $t^{est}_{ign} \approx 1 + \tau^*_e/\tau^*_f + \tau^*_{0D}/\tau^*_f$, i.e., the sum of convective, evaporative and ignition non-dimensional time scales. Here, τ^*_e is a characteristic droplet evaporation time and τ^*_{0D} is the ignition delay time of a homogeneous adiabatic isobaric reactor at $\phi = \phi_0$ and $T^*_u = T^*_w \approx T^*_e$. For the range of T_e and Da considered in this study, $\tau^*_{0D}/\tau^*_f \lesssim 0.1$. We can define an *evaporation* Damköhler number $\mathrm{Da}_e = \tau^*_f/\tau^*_e$, and use the definition of St to obtain $\mathrm{Da}_e = \frac{1}{\mathrm{St}}\frac{\tau^*_{d,0}}{\tau^*_e}$. From Eq. (3f), we can approximate $\tau^*_e \sim \frac{3\mathrm{Sc}}{\mathrm{Sh}}\frac{\tau^*_{d,0}}{H_M}$, from which it follows that $\mathrm{Da}_e \sim \frac{1}{\mathrm{St}}$ and that Da_e is independent of Da. This shows that the choice of $\mathrm{St} \ll 1$ directly affects how close to the wall the spray will reach prior to fully evaporating. Since $\tau^*_e/\tau^*_f = 1/\mathrm{Da}_e \sim \mathrm{St}$, for constant St, T_e and ϕ_0, linear coupling would result in a near-constant t^{est}_{ign} with respect to Da. The up to four-fold increase in t_{ign} observed in the range of Da considered in Fig. 8a and its commensurately high permutation importance is thus evidence of the highly non-linear coupling of the multiphase physics in the present configuration.

Figure 8b demonstrates the parametric behavior of ϕ_{ign} and shows that the ignition kernel composition is nearly independent of both St and ϕ_0. Both parameters have permutation importances substantially lower than Da and T_e. This is an interesting result, since ϕ_0 determines the total fuel availability and St directly affects the rate at which liquid fuel is converted to vapor and deposited in the gas phase. The figure also shows that ϕ_{ign} is nearly independent of Da. It remains at a constant fuel-lean value until the ignition limit is approached, where it increases substantially, as was also seen in Fig. 7c.

In analyzing results for all cases in which ignition occurred, we find that $0.04 < x_{ign}/x_F < 0.76$. This key aspect of the ignition phenomenology discussed in Section 4.1 is thus found to be consistent across the entirety of the parameter range considered, namely that ignition occurs at locations $x_{ign} < x_F$ and compositions $\phi_{ign} < \phi_F$. Furthermore, we find that x_F consistently delineates an upstream non-premixed region from a premixed region between x_F and the wall. Initial flame kernel formation and propagation is found to occur consistently in the latter region, which was explained through consideration of the most reactive mixture in the context of Fig. 4.

We find in Fig. 8c that x_{ign} is nearly independent of ϕ_0, except at the highest Da considered where a reduction in ϕ_0 is found to result in a moderate increase in x_{ign}. In a dimensional setting, an increase in strain rate would be expected to cause ignition kernels to form nearer to the wall, with the first-order effect of increased strain being the reduction of the boundary layer thickness within which ignition kernels have been shown to form. In the present non-dimensional formulation, this first-order effect is accounted for, resulting in $\delta \approx 2.0$ as noted above. However, as was also seen in Fig. 7c, x_{ign} is still found to vary substantially with Da. In Fig. 8c, we show the estimated steady-state thermal boundary-layer thickness $\delta_T \approx 2.0\mathrm{Pr}^{0.4}$ using a black dashed line, as derived for non-reacting, constant property flows [25]. An estimate of non-dimensional laminar flame thickness is made by considering a laminar premixed flame with $T^*_u = T^*_0$ and $\phi = 1.0$ and computing $\delta^*_F \approx (T^*_{ad} - T^*_0)/\max(\partial T^*/\partial x^*)$ [51]. The non-dimensional thickness $\delta_F = \delta^*_F/\ell^*$ is shown in the figure using a black dash-dotted line. At high Da, ignition kernel formation is seen to occur near the edge of the thermal boundary layer, particularly for higher values of T_e. However, at lower Da and up to the ignition limit, x_{ign} reduces and is seen to approach a value near δ_F. We thus find in the present case that ignition kernels, which consistently form in a premixed region, do not form closer to the wall than the order of the flame thickness, with lower Da instead ultimately resulting in the system becoming non-igniting. Considering the flame-wall interaction literature for head-on quenching premixed laminar flames propagating into isothermal walls, these have been shown to quench at $\mathrm{Pe}_{\delta_F} \sim 1$ [52,53] with $\mathrm{Pe}_{\delta_F} \equiv x/\delta_F$ as a quenching Peclet number, indicating that for isothermal walls flames cannot propagate closer than the order of the laminar flame thickness. We find, therefore, that only in the low-Da regime near the ignition limit does the location of ignition kernel formation in HSI exhibit similar behavior to that of the quenching distance in a head-on quenching configuration; in the high-Da regime, it conforms more closely to the thermal boundary layer, and there exists a transition region between these regimes for intermediate values of Da.

4.4. Comparison to theory

It was noted in Section 1 that the problem of HSI has been studied theoretically using matched-asymptotic analysis. Here, we consider the ignition criterion of Kats and Greenberg [7] for a two-phase stagnating flow and compare it to the simulation results of this study. Since it is derived from the steady-state equations, this theoretical criterion cannot provide information regarding t_{ign} or other unsteady behavior, but does provide a prediction of the parametric dependencies of the ignition limit. The nature of the discussion in this section is restricted to being qualitative [8] due to the number of simplifying assumptions made in the development of the theoretical criterion in order to maintain an analytically tractable formulation that are not made in the numerical simulations, including the use of one-step global Arrhenius chemistry and a constant droplet evaporation rate. In producing the theoretical results, we consider an activation energy of $E^*_a = 2.0 \times 10^5$ J/mol and a pre-exponential constant of $A^* = 1.0 \times 10^{10}\,\mathrm{s}^{-1}$ to approximate the behavior of large alkanes undergoing stoichiometric combustion at atmospheric pressure [54].

We noted in Section 4.1 that we can approximate a characteristic droplet evaporation time from Eq. (3f) as $\tau^*_e \sim \frac{3\mathrm{Sc}}{\mathrm{Sh}}\frac{\tau^*_{d,0}}{H_M}$. Approximating the evaporation rate as $C^* \sim 1/\tau^*_e$, we can express the evaporation Damköhler number introduced in Section 4.3 as $\mathrm{Da}_e = \tau^*_f/\tau^*_e \sim C^*/a^*$. Since we showed previously that $\mathrm{Da}_e \sim 1/\mathrm{St}$, the effect of the parametric variation of St on the ignition limit in the present study can thus be compared to the inverse variation in Da_e in the theoretical criterion. We show that this is indeed the case in Fig. 9. For a constant ϕ_0 and St, both the simulation results and theoretical criterion yield a near-linear ignition limit when plotted on log-linear axes for the parameter ranges shown. The simulation results show that an increase in St results in a contraction of the ignition limit, as discussed in Section 4.3. The theoretical criterion predicts that a reduction in Da_e also results in a contraction of the ignition limit. This is in agreement with the

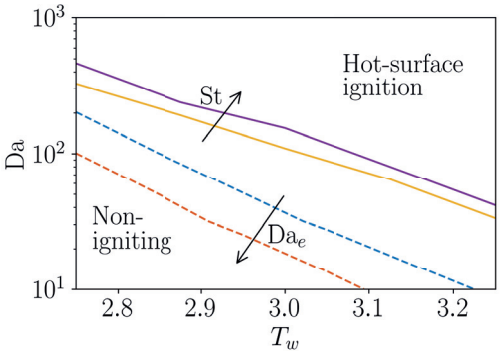

Fig. 9. Qualitative comparison of ignition limit parametric dependencies for $\phi_0 = 1.0$. Solid lines: present numerical study, St = 0.01 ——, St = 0.1 ——; dashed lines: solution of the theoretical criterion of Kats and Greenberg [7], $Da_e = 2.0$ - - -, $Da_e = 4.0$ - - -.

foregoing analysis, since within the approximations of the theoretical criterion, a reduction in Da_e is proportional to an increase in St. The relationship between Da_e in the theoretical criterion and St in the simulations is not quantitative, however, since in the theoretical formulation Da_e enforces a constant evaporation rate throughout the domain. By contrast, St is defined based on the inflow condition in the simulations, but droplet diameters, temperatures and evaporation rates (and thus local Stokes numbers) are allowed to vary across time and space to conform to the gas phase. Thus, although a reduction in Da_e is expected to have the same qualitative effect on the theoretical ignition limit as that of an increase in St on the numerically-obtained limit, the magnitudes of these changes are not quantitatively comparable, as seen in Fig. 9.

The qualitative agreement between the theoretical and numerical models indicates that within the parameter ranges considered, the assumptions used to derive the theoretical criterion are reasonable and preserve many of the key parametric dependencies of the ignition limit. This lends credence to the use of such techniques for the analysis of limit phenomena in spray combustion and for developing an understanding of the underlying physical processes. However, even within the limits of a qualitative comparison, a steady-state theoretical formulation cannot recover important information regarding unsteady behavior, including the ignition delay time, location and local composition discussed in Section 4.1,4.3, for which the present unsteady numerical formulation employing detailed models for chemistry and evaporation is needed.

5. Conclusions

HSI of a wall-impinging fuel spray was analyzed using an unsteady one-dimensional formulation. The chemical source terms were modeled using finite-rate chemistry with a realistic chemical mechanism for *n*-dodecane/air combustion and spray evaporation was considered using a non-equilibrium model. The present study demonstrates the system dynamics leading to ignition, recovers spatio-temporal and chemical details of ignition kernel formation and precludes ambiguities due to possible solution bifurcations which arise in steady-state formulations. The configuration considered is relevant to the safety of industrial systems, namely that of the accidental leakage of a pressurized fuel line near a hot surface. Through non-dimensionalization of the governing equations, we identified the following key controlling parameters: Damköhler number based on the global strain rate, wall temperature, inflow Stokes number, and inflow total equivalence ratio.

By analyzing the phenomenology of the unsteady processes leading to ignition in the present configuration, we showed that spray evaporation resulted in the formation of non-premixed and premixed regions within the domain, identified using the Takeno index. We found that ignition occurred in the high-temperature region near the wall, at a location $0 < x_{ign} < x_F$ and composition $\phi_{ign} < \phi_F$, corresponding to a premixed region. Our analysis showed that the location and composition at which ignition occurred were due to the most reactive mixture lying at all times prior to ignition at a location $x < x_F$ because of the combined effects of convection and spray evaporation. We found that the temporal peak in the wall heat flux resulted from the quenching of a downsteam-propagating flame after ignition. Another flame simultaneously propagated upstream into the fuel spray, resulting in saturated droplet temperatures and increased evaporation rates which sustained the flame.

The importance of the non-dimensional parameters considered in determining the ignition limit, t_{ign}, x_{ign} and ϕ_{ign} was shown quantitatively by analyzing the permutation importances obtained from random forest classifiers and regressors trained on the simulation data. It was found that the ignition limit contracted and shifted toward richer ϕ_0 and higher T_e at lower Da. Although reduction of St by an order of magnitude only resulted in a small expansion of the limit, this result is influenced by the present formulation's assumption that droplets follow gas-phase streamlines; this assumption should be relaxed and its implications considered in future studies. The ignition kernel composition was found to be nearly independent of the inlet composition, and was determined primarily by T_e. We also showed that x_{ign} was bounded by the extent of the thermal boundary-layer thickness δ_T, reaching a near-constant minimum value on the order of the premixed flame thickness at low Da near the ignition limit. In comparing our results to the qualitative HSI regime diagram proposed in the experimental literature, we quantified the notion of 'ideality' of conditions for HSI of wall-impinging fuel sprays across broad ranges of the controlling parameters.

We compared the results of the present study for the parametric behavior of the ignition limit to those of a recent matched asymptotic study. Qualitative agreement was achieved for the parametric dependence of the ignition limit on Da and T_e, and the effect of St was shown to be reasonably approximated by an evaporation Damköhler number. The comparison highlighted the importance of the present numerical simulations to study the unsteady dynamics and the details of the HSI process. The code developed and used in this study is publicly available through our GitHub repository: https://github.com/IhmeGroup/sprayHSI

Declaration of Competing Interest

The authors declare that they have no known competing financial interests or personal relationships that could have appeared to influence the work reported in this paper.

Acknowledgments

Financial support from The Boeing Company under grant number 134708 [IC2017-2182] is gratefully acknowledged. DM acknowledges the Natural Sciences and Engineering Research Council of Canada [PGSD2-532767-2019]. This research used resources of the National Energy Research Scientific Computing Center, a U.S. Department of Energy Office of Science User Facility operated under Contract No. DE-AC02-05CH11231. Dr. Gershon Kats and Prof. Barry Greenberg are thanked for fruitful discussions regarding their theoretical ignition criterion.

References

[1] J.D. Colwell, A. Reza, Hot surface ignition of automotive and aviation fluids, Fire Technol. 41 (2) (2005) 105–123, doi:10.1007/s10694-005-6388-6.

[2] ASTM, ASTM-E659: Standard Test Method for Autoignition Temperature of Liquid Chemicals, 2005,
[3] S. Davis, D. Chavez, H. Kytomaa, Hot surface ignition of flammable and combustible liquids, SAE Paper 2006-01-1014, 2006, doi:10.4271/2006-01-1014.
[4] M.S. Ulcay, L. Dillard, J.P. Gore, Emperical modeling of minimum hot surface ignition temperature for aviation fluids, AIAA Paper 2019-4458, 2019.
[5] A. Johnson, A. Roth, N. Moussa, Hot surface ignition tests of aircraft fluids, Technical Report, Air Force Wright Aeronautical Laboratory, 1988. Accession No. ADA207372
[6] C.K. Law, On the stagnation-point ignition of a premixed combustible, Int. J. Heat Mass Transf. 21 (11) (1978) 1363–1368, doi:10.1016/0017-9310(78)90199-0.
[7] G. Kats, J.B. Greenberg, Stagnation-point spray flame ignition by an isothermal surface, J. Eng. Math. 110 (1) (2018) 181–194, doi:10.1007/s10665-017-9947-1.
[8] G. Kats, J.B. Greenberg, Stagnation-point polydisperse spray flame ignition, Combust. Theor. Model. 23 (5) (2019) 771–797, doi:10.1080/13647830.2019.1589580.
[9] S.K. Aggarwal, W.A. Sirignano, Ignition of fuel sprays: deterministic calculations for idealized droplet arrays, Symp. (Int.) Combust. 20 (1) (1985) 1773–1780, doi:10.1016/S0082-0784(85)80674-3.
[10] S.K. Aggarwal, W.A. Sirignano, Ignition of polydisperse sprays: importance of D20, Combust. Sci. Technol. 46 (3–6) (1986) 289–300, doi:10.1080/00102208608959804.
[11] S.K. Aggarwal, Chemical-kinetics modeling for the ignition of idealized sprays, Combust. Flame 69 (3) (1987) 291–302, doi:10.1016/0010-2180(87)90122-2.
[12] M. Lee, Y. Fan, Y. Ju, Y. Suzuki, Ignition characteristics of premixed cool flames on a heated wall, Combust. Flame 231 (2021), doi:10.1016/j.combustflame.2021.111476.
[13] D. Mohaddes, P. Boettcher, M. Ihme, Hot surface ignition of a wall-impinging fuel spray: modeling and analysis using large-eddy simulation, Combust. Flame 228 (2021) 443–456, doi:10.1016/j.combustflame.2021.02.025.
[14] N.M. Laurendeau, Thermal ignition of methane-air mixtures by hot surfaces: a critical examination, Combust. Flame 46 (C) (1982) 29–49, doi:10.1016/0010-2180(82)90005-0.
[15] X. Song, L.D. Schmidt, R. Aris, The ignition criteria for stagnation-point flow: Semenov-Frank-Kamenetski or van't Hoff, Combust. Sci. Technol. 75 (4–6) (1991) 311–331, doi:10.1080/00102209108924094.
[16] C.G. Fotache, T.G. Kreutz, D.L. Zhu, C.K. Law, An experimental study of ignition in nonpremixed counterflowing hydrogen versus heated air, Combust. Sci. Technol. 109 (1–6) (1995) 373–393, doi:10.1080/00102209508951910.
[17] W.J. Sheu, C.J. Sun, Ignition delay of non-premixed stagnation-point flows, Int. J. Heat Mass Transf. 45 (17) (2002) 3549–3558, doi:10.1016/S0017-9310(02)00069-8.
[18] L.L. Kirkbey, R.A. Schmitz, An analytical study of the stability of a laminar diffusion flame, Combust. Flame 10 (3) (1966) 205–220, doi:10.1016/0010-2180(66)90077-0.
[19] D. Vlachos, L. Schmidt, R. Aris, Ignition and extinction of flames near surfaces: combustion of H_2 in air, Combust. Flame 95 (3) (1993) 313–335, doi:10.1016/0010-2180(93)90135-P.
[20] A. Vié, B. Franzelli, Y. Gao, T. Lu, H. Wang, M. Ihme, Analysis of segregation and bifurcation in turbulent spray flames: a 3D counterflow configuration, Proc. Combust. Inst. 35 (2) (2015) 1675–1683, doi:10.1016/J.PROCI.2014.06.083.
[21] W. Xie, P.B. Govindaraju, Z. Ren, M. Ihme, Structural analysis and regime diagrams of laminar counterflow spray flames with low-temperature chemistry, Proc. Combust. Inst. 38 (September) (2021) 3193–3200, doi:10.1016/j.proci.2020.06.274.
[22] G. Stahl, J. Warnatz, Numerical investigation of time-dependent properties and extinction of strained methane and propane-air flamelets, Combust. Flame 85 (3–4) (1991) 285–299, doi:10.1016/0010-2180(91)90134-W.
[23] R. Kee, M. Coltrin, P. Glarborg, Chemically Reacting Flow: Theory & Practice, John Wiley & Sons, Inc., 2003.
[24] A.E. Long, R.L. Speth, W.H. Green, Ember: an open-source, transient solver for 1D reacting flow using large kinetic models, applied to strained extinction, Combust. Flame 195 (2018) 105–116, doi:10.1016/j.combustflame.2018.05.001.
[25] F.M. White, Viscous Fluid Flow, McGraw-Hill, 2011.
[26] G. Continillo, W.A. Sirignano, Counterflow spray combustion modeling, Combust. Flame 81 (3–4) (1990) 325–340, doi:10.1016/0010-2180(90)90029-Q.
[27] B. Franzelli, B. Fiorina, N. Darabiha, A tabulated chemistry method for spray combustion, Proc. Combust. Inst. 34 (1) (2013) 1659–1666, doi:10.1016/j.proci.2012.06.013.
[28] R. Miller, K. Harstad, J. Bellan, Evaluation of equilibrium and non-equilibrium evaporation models for many-droplet gas-liquid flow simulations, Int. J. Multiphas. Flow 24 (6) (1998) 1025–1055, doi:10.1016/S0301-9322(98)00028-7.
[29] J. Ferry, S. Balachandar, A fast Eulerian method for disperse two-phase flow, Int. J. Multiphas. Flow 27 (7) (2001) 1199–1226, doi:10.1016/S0301-9322(00)00069-0.
[30] P.C. Ma, H. Wu, T. Jaravel, L. Bravo, M. Ihme, Large-eddy simulations of transcritical injection and auto-ignition using diffuse-interface method and finite-rate chemistry, Proc. Combust. Inst. 37 (3) (2019) 3303–3310, doi:10.1016/j.proci.2018.05.063.
[31] T. Yao, Y. Pei, B.-J. Zhong, S. Som, T. Lu, K.H. Luo, A compact skeletal mechanism for n-dodecane with optimized semi-global low-temperature chemistry for diesel engine simulations, Fuel 191 (2017) 339–349, doi:10.1016/J.FUEL.2016.11.083.
[32] H. Wang, X. You, A.V. Joshi, S.G. Davis, A. Laskin, F. Egolfopoulos, C.K. Law, USC mech version II: high-temperature combustion reaction model of H2/CO/C1-C4 compounds, 2007, http://ignis.usc.edu/USC_Mech_II.htm
[33] D. Mohaddes, W. Xie, M. Ihme, Analysis of low-temperature chemistry in a turbulent swirling spray flame near lean blow-out, Proc. Combust. Inst. 38 (2021) 3435–3443, doi:10.1016/j.proci.2020.08.030.
[34] A.C. Hindmarsh, P.N. Brown, K.E. Grant, S.L. Lee, R. Serban, D.E. Shumaker, C.S. Woodward, SUNDIALS: suite of nonlinear and differential/algebraic equation solvers, ACM Trans. Math. Softw. (TOMS) 31 (3) (2005) 363–396.
[35] E. Radenac, J. Gressier, P. Millan, Methodology of numerical coupling for transient conjugate heat transfer, Comput. Fluids 100 (2014) 95–107, doi:10.1016/j.compfluid.2014.05.006.
[36] D.G. Goodwin, R.L. Speth, H.K. Moffat, B.W. Weber, Cantera: an object-oriented software toolkit for chemical kinetics, thermodynamics, and transport processes, 2017, (https://www.cantera.org).Version 2.4.0. 10.5281/zenodo.170284
[37] A. Wehrfritz, H. Wang, E.R. Hawkes, Y. Gao, T. Lu, Wall-impinging laminar premixed n-dodecane flames under autoignitive conditions, Proc. Combust. Inst. 37 (2) (2019) 1647–1654, doi:10.1016/J.PROCI.2018.06.118.
[38] R. Bilger, S. Stårner, R. Kee, On reduced mechanisms for methane-air combustion in nonpremixed flames, Combust. Flame 80 (2) (1990) 135–149, doi:10.1016/0010-2180(90)90122-8.
[39] E. Mastorakos, T.A. Baritaud, T.J. Poinsot, Numerical simulations of autoignition in turbulent mixing flows, Combust. Flame 109 (1–2) (1997) 198–223, doi:10.1016/S0010-2180(96)00149-6.
[40] Y. Pei, E.R. Hawkes, M. Bolla, S. Kook, G.M. Goldin, Y. Yang, S.B. Pope, S. Som, An analysis of the structure of an n-dodecane spray flame using TPDF modelling, Combust. Flame 168 (2016) 420–435, doi:10.1016/J.COMBUSTFLAME.2015.11.034.
[41] H. Yamashita, M. Shimada, T. Takeno, A numerical study on flame stability at the transition point of jet diffusion flames, Symp. (Int.) Combust. 26 (1) (1996) 27–34, doi:10.1016/S0082-0784(96)80196-2.
[42] F. Shum-Kivan, J. Marrero Santiago, A. Verdier, E. Riber, B. Renou, G. Cabot, B. Cuenot, Experimental and numerical analysis of a turbulent spray flame structure, Proc. Combust. Inst. 36 (2) (2017) 2567–2575, doi:10.1016/j.proci.2016.06.039.
[43] A. Rezchikova, C. Mehl, S. Drennan, O. Colin, Large eddy simulation of a turbulent spray burner using thickened flame model and adaptive mesh refinement, J. Eng. Gas Turb. Power 143 (4) (2021) 1–8, doi:10.1115/1.4049827.
[44] A. Dreizler, B. Böhm, Advanced laser diagnostics for an improved understanding of premixed flame-wall interactions, Proc. Combust. Inst. 35 (1) (2015) 37–64, doi:10.1016/j.proci.2014.08.014.
[45] L. Breiman, Random forests, Mach. Learn. 45 (2001) 5–32, doi:10.1023/A:1010933404324.
[46] W.T. Chung, A.A. Mishra, N. Perakis, M. Ihme, Data-assisted combustion simulations with dynamic submodel assignment using random forests, Combust. Flame 227 (2021) 172–185 2009.04023, doi:10.1016/j.combustflame.2020.12.041.
[47] E. Gutheil, W.A. Sirignano, Counterflow spray combustion modeling with detailed transport and detailed chemistry, Combust. Flame 113 (1–2) (1998) 92–105, doi:10.1016/S0010-2180(97)00192-2.
[48] R. Seiser, H. Pitsch, K. Seshadri, W.J. Pitz, H.J. Curran, Extinction and autoignition of n-heptane in counterflow configuration, Proc. Combust. Inst. 28 (2000) 2029–2037.
[49] S. Liu, J.C. Hewson, J.H. Chen, Nonpremixed n-heptane autoignition in unsteady counterflow, Combust. Flame 145 (4) (2006) 730–739, doi:10.1016/j.combustflame.2006.01.011.
[50] S. Xie, Z. Lu, Z. Chen, Effects of strain rate and Lewis number on forced ignition of laminar counterflow diffusion flames, Combust. Flame 226 (December) (2021) 302–314, doi:10.1016/j.combustflame.2020.12.027.
[51] C. Hasse, M. Bollig, N. Peters, H.A. Dwyer, Quenching of laminar iso-octane flames at cold walls, Combust. Flame 122 (1–2) (2000) 117–129, doi:10.1016/S0010-2180(00)00107-3.
[52] S.R. Vosen, R. Greif, C.K. Westbrook, Unsteady heat transfer during laminar flame quenching, Symp. (Int.) Combust. 20 (1) (1985) 75–83, doi:10.1016/S0082-0784(85)80490-2.
[53] M. Mann, C. Jainski, M. Euler, B. Böhm, A. Dreizler, Transient flame-wall interactions: experimental analysis using spectroscopic temperature and CO concentration measurements, Combust. Flame 161 (9) (2014) 2371–2386, doi:10.1016/j.combustflame.2014.02.008.
[54] C.K. Westbrook, F.L. Dryer, Simplified reaction mechanisms for the oxidation of hydrocarbon fuels in flames, Combust. Sci. Technol. 27 (1–2) (1981) 31–43, doi:10.1080/00102208108946970.